AGU PUBLICATIONS

JGR

Journal of Geophysical Research: Earth Surface

RESEARCH ARTICLE
10.1002/2015JF003467

Key Points:
- PLFs of uncertain origin were discovered on the South Kara Sea shelf
- Anomalous concentrations of biogenic methane correspond to one of the PLFs
- Subpermafrost methane accumulations can lead to the formation of PLFs

Correspondence to:
P. Serov,
pavel.russerov@uit.no

Citation:
Serov, P., A. Portnov, J. Mienert, P. Semenov, and P. Ilatovskaya (2015), Methane release from pingo-like features across the South Kara Sea shelf, an area of thawing offshore permafrost, *J. Geophys. Res. Earth Surf.*, *120*, 1515–1529, doi:10.1002/2015JF003467.

Received 30 JAN 2015
Accepted 11 JUL 2015
Accepted article online 16 JUL 2015
Published online 7 AUG 2015

Methane release from pingo-like features across the South Kara Sea shelf, an area of thawing offshore permafrost

Pavel Serov[1,2], Alexey Portnov[1,2], Jurgen Mienert[1], Peter Semenov[2], and Polina Ilatovskaya[2]

[1]Centre for Arctic Gas Hydrate, Environment and Climate, Department of Geology, UiT The Arctic University of Norway, Tromsø, Norway, [2]I.S. Gramberg VNIIOkeangeologia, Saint Petersburg, Russia

Abstract The Holocene marine transgression starting at ~19 ka flooded the Arctic shelves driving extensive thawing of terrestrial permafrost. It thereby promoted methanogenesis within sediments, the dissociation of gas hydrates, and the release of formerly trapped gas, with the accumulation in pressure of released methane eventually triggering blowouts through weakened zones in the overlying and thinned permafrost. Here we present a range of geophysical and chemical scenarios for the formation of pingo-like formations (PLFs) leading to potential blowouts. Specifically, we report on methane anomalies from the South Kara Sea shelf focusing on two PLFs imaged from high-resolution seismic records. A variety of geochemical methods are applied to study concentrations and types of gas, its character, and genesis. PLF 1 demonstrates ubiquitously low-methane concentrations (14.2–55.3 ppm) that are likely due to partly unfrozen sediments with an ice-saturated internal core reaching close to the seafloor. In contrast, PLF 2 reveals anomalously high-methane concentrations of >120,000 ppm where frozen sediments are completely absent. The methane in all recovered samples is of microbial and not of thermogenic origin from deep hydrocarbon sources. However, the relatively low organic matter content (0.52–1.69%) of seafloor sediments restricts extensive in situ methane production. As a consequence, we hypothesize that the high-methane concentrations at PLF 2 are due to microbial methane production and migration from a deeper source.

1. Introduction

During the ice ages of late Pleistocene [*Jakobsson et al.*, 2014] a thick layer of permafrost and gas hydrate deposits formed in subaerial conditions on the Arctic shelves [*Khimenkov and Brushkov*, 2003]. Following the Last Glacial Maximum (LGM) (~19 ka) [*Aubry et al.*, 2009] Arctic shelves were flooded during an extensive ocean transgression reaching ~120 m [*Bauch et al.*, 2001]. Relatively warm ocean waters encroached on areas which had formerly been coastal planes [*Fairbanks*, 1989; *Fleming et al.*, 1998], thereby initiating thermal inundation of permafrost from the top [*Osterkamp et al.*, 1989; *Paull et al.*, 2007]. Simultaneously, permafrost thawed from the bottom due to the influence of geothermal heat flux coupled with warmer upper boundary conditions [*Nicolsky et al.*, 2012; *Rokos et al.*, 2009].

Permafrost can be considered an impermeable seal for gas [e.g., *Shakhova et al.*, 2010] or at least a layer substantially reducing gas migration from the subsurface [*Yakushev*, 2009]. Thus, the distribution and decay of Arctic permafrost over both long- and short-time periods provides an important control on natural emissions of gas, including the potent greenhouse gas—methane—to the atmosphere [*Shakhova et al.*, 2010]. Thawing subsea permafrost also triggers a significant release of methane of various origins that migrates through open taliks into the shallow seas and atmosphere, thereby affecting the global climate [*Delisle*, 2000; *Frederick and Buffett*, 2014; *Majorowicz et al.*, 2011; *Nicolsky et al.*, 2012; *Romanovskii et al.*, 2005].

The extent of relict subsea permafrost along with an inventory of the associated gas hydrates stored within and below the permafrost on the Arctic shelves is still controversial [*Collett et al.*, 2011; *Rachold et al.*, 2007; *Yakushev*, 2009]. Numerous studies have improved our knowledge base and extended the subsea permafrost mapping on the Beaufort Sea shelf [*Brothers et al.*, 2012; *Hu et al.*, 2013; *Taylor et al.*, 2013], the Laptev and East Siberian Sea shelves [*Nicolsky et al.*, 2012; *Romanovskii et al.*, 1998, 2004], and the Kara Sea shelf [*Portnov et al.*, 2013; *Rekant et al.*, 2005; *Rekant and Vasiliev*, 2011]. Modeling performed by *Romanovskii et al.* [2004] suggests that a continuous permafrost layer extended to the 60 m isobaths in the

Laptev and East Siberian Seas. However, continuous subsea permafrost appears to be less abundant on the other Arctic coastal shelf areas. *Brothers et al.* [2012] concluded that minimal extent of ice-bearing permafrost on the U.S. Beaufort continental shelf is limited to the 20 m isobaths.

Portnov et al. [2013] mapped a region of extensive gas release over an area of at least 7500 km^2 located in the South Kara Sea in water depths >20 m. The presence of individual gas flares and gas fronts within the water column is closely related to thawed permafrost boundaries. Permafrost was present in only 15% of boreholes drilled offshore Yamal Peninsula in water depths >20 m [*GEOS*, 1997]. These drilling results and observations of gas expulsion within the water column imply that the South Kara Sea is a key area of ongoing and extensive permafrost decay.

There are two competing hypotheses for the conditions under which pingo-like formations (PLFs) form: (1) an early study suggests that they formed under terrestrial conditions in low relative sea level stands during glacial episodes throughout the late Pleistocene and were subsequently submerged in interglacials [*Shearer et al*., 1971] or, alternatively, (2) that they developed in marine environments after the shelf flooding in Holocene times [*Bondarev et al*., 2002; *Paull et al*., 2007]. Earlier models of marine PLF formation speculated that gas, emitted during dissociation of gas hydrates within and below thawing permafrost, built up at high pressures driving seafloor doming [*Paull et al*., 2007]. However, the debate is still ongoing as to whether PLFs are related to gas release since many of the documented PLFs do not reveal any measurable gas discharge [*Bondarev et al*., 2002; *Paull et al*., 2007].

Steady state gas leakage and even blowout events have been documented from some of the PLFs at the Beaufort Sea and Russian Arctic shelves [*Hovland et al*., 1993; *Judd and Hovland*, 2007]. Noteworthy, a drilling vessel (operated by "AMIGE" company) experienced an emergency situation due to sudden and extensive gas release from a well after the drill bit penetrated a gas pocket inside a large PLF in the Pechora Sea [*Bondarev et al*., 2002; *Rokos*, 2008]. Hence, it follows that some PLFs act as major gas storage and seepage hot spots. The recently described Siberian craters found onshore in permafrost regions of the Yamal Peninsula have also been speculated to be the result of accumulation of high gas pressure and abrupt methane release [*Bogoyavlenskiy*, 2014a, 2014b; *Moskvitch*, 2014].

This study concentrates on offshore PLFs in the shallow waters of the South Kara Sea. Here we report on the acoustic, geological, and geochemical evidence revealing the genesis and evolution of the observed PLFs. We apply a number of geochemical methods, including gas chromatography of gaseous and high molecular weight (HMW) hydrocarbons as well as methane isotope measurements of carbon and hydrogen for deciphering the origin of gas in bottom sediments above two characteristic PLFs in the South Kara Sea shelf. We also integrate our results of both geochemical and high-resolution seismic (HRS) studies with a modeled evolution of permafrost [*Rokos et al*., 2009] allowing us to suggest possible scenarios for the formation of PLFs on the South Kara Sea shelf.

2. Geological Setting

2.1. Tectonic Framework, Seafloor Morphology, and Lithology of Bottom Sediments

The South Kara Sea lies in a large tectonic depression, the South Kara Syncline, located to the west of the Yamal Peninsula. The syncline developed at a continuation of the East Siberian Plate neighboring the North Kara Plate located to the north of the Novaya Zemlya Archipelago [*Stupakova*, 2011]. The South Kara Syncline has a Paleozoic basement and an up to 14 km thick Permian-Cenozoic sedimentary cover composed of terrigenous deposits. Pliocene-Quaternary strata unconformably overlay older deposits reaching maximal thickness of 300 m on the Yamal Peninsula and ~125 m on the West Yamal shelf [*Sherbakov et al*., 2010].

The Novozemelsky trough and coastal shelf offshore Yamal Peninsula are the two major physiographic elements that define the morphology of the South Kara Sea (Figure 1a). Shelf depths of less than 120 m extend up to 200 km offshore in the central part and up to 105 km and 170 km in the southern and northern parts of the Kara Sea, respectively. The coastal shelf of the South Kara Sea is glacially eroded [*Melnikov and Spesivtsev*, 1995; *Pavlidis et al*., 1998] with overdeepened troughs and incised river valleys partly filled with marine terrigenous deposits [*Sherbakov et al*., 2010].

The upper sedimentary units across the shelf are dominated by Pleistocene and Holocene marine and alluvial-marine deposits. Pre-Weichselian deposits consist mostly of clays overlain by interbeds of sands,

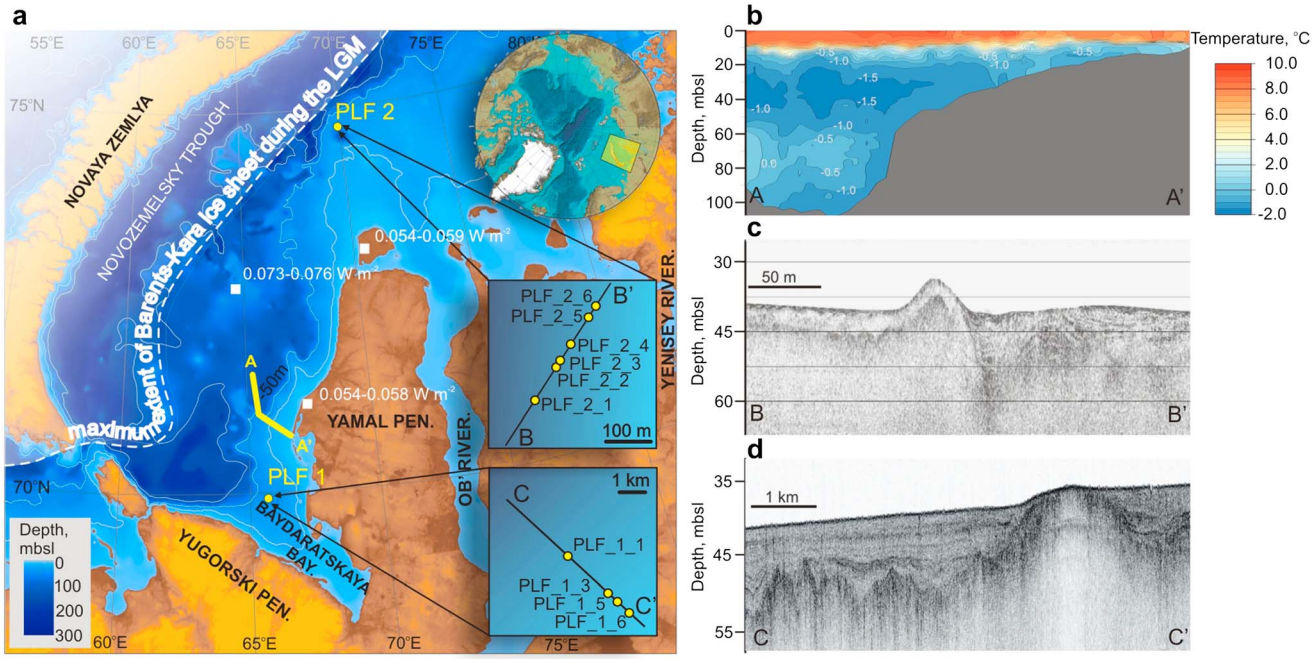

Figure 1. (a) Location of sampling sites on the South Kara Sea shelf. The dashed white line shows the maximum extent of Barents-Kara ice sheet coming from the west during the Late Glacial Maximum (modified from *Polyak et al.* [2002]). The solid yellow line shows the location of water temperature profile obtained by I.S. Gramberg VNIIOkeangeologia in summer 2013. The white squares show the locations of boreholes, where the heat flux values were obtained. The insets in Figure 1a show the location of high-resolution seismic lines crossing the PLFs and sampling stations (yellow dots). (b) Water temperature profile. (c) High-resolution seismic line across the PLF 2. (d) High-resolution seismic line across the PLF 1.

silts, and clays of Middle Weichselian to Holocene age (marine oxygen isotope stage (MIS)4-MIS1) [*Melnikov and Spesivtsev*, 1995]. The uppermost Holocene sediments consist of mud with low sand content and scarce ice-rafted debris [*Levitan et al.*, 2004; *Stein et al.*, 2004]. Holocene sedimentation is facilitated by the vigorous sediment deposition from rivers and extensive coastal erosion. The most rapid sedimentation and highest sedimentation rates occur at the outer northwestern part of the Baydratskaya Bay and at the estuaries of the Ob' and Enisey Rivers (average linear Holocene sedimentation rates are ~135 cm/kyr and 27–159 cm/kyr, respectively) [*Polyak et al.*, 2000; *Stein et al.*, 2004].

2.2. Permafrost Settings and Gas Hydrate Stability

Reconstructions of the Barents-Kara ice sheet extent reveal that a large part of the South Kara Sea shelf was ice-free and exposed to subaerial conditions during the Late Weichselian [*Polyak et al.*, 2008; *Svendsen et al.*, 2004] (Figure 1a). The sustained cold temperatures to −20°C that prevailed over this extended period [*Romanovskii et al.*, 2003] led to extensive and deep permafrost generation. Drilling results indicate the presence of a more than 300 m thick permafrost layer onshore Yamal Peninsula [*Melnikov and Spesivtsev*, 1995]. Subsea permafrost was discovered in individual boreholes of the South Kara Sea in water depth of up to 115 m. Modeling of permafrost generation at the South Kara Sea shelf suggests that a 275–480 m thick permafrost layer occurred during the LGM [*Portnov et al.*, 2014; *Rokos et al.*, 2009]. Such sustained, frozen temperatures provide ideal conditions for the formation of gas hydrates within and beneath the permafrost where methane is present (Figure 2) [*Collett et al.*, 2011; *Ruppel*, 2007].

Holocene flooding of the South Kara Sea shelf provoked melting of subsea permafrost (Figure 2) [*Rokos and Tarasov*, 2007]. Models of subsea permafrost evolution suggest a permafrost thickness reduction by 51–100% over a 10.5 kyr period of submergence (Figure 2). Complete melting of submerged permafrost under relatively cold water conditions (−0.5°C) requires 10.4–20.4 kyr, dependent on the geothermal heat flux and thermal conductivities of the soils and sediments [*Portnov et al.*, 2014; *Rokos et al.*, 2009].

In the South Kara Sea, summer water temperature below the thermocline is usually ≤−0.5°C [*GEOS*, 1997; *Portnov et al.*, 2013]. Conductivity-temperature-depth measurements (performed by I.S.Gramberg VNIIOkeangeologia)

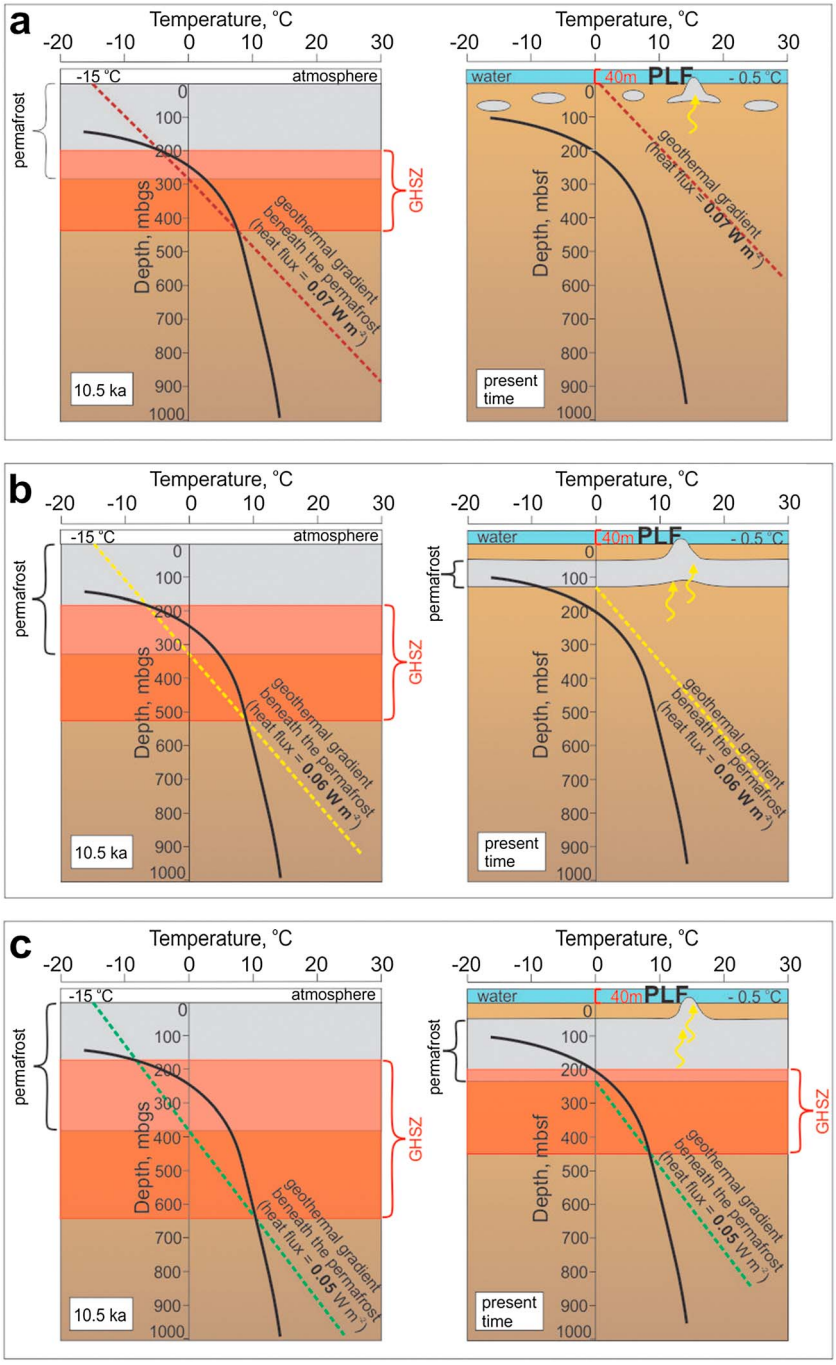

Figure 2. Scenarios of permafrost and GHSZ evolution of the South Kara Sea shelf in 40 m water depth for 10.5 ka and present time. The term ka relates to thousand years before present [*Aubry et al.*, 2009]. The black curves show the phase boundary for pure methane hydrate (~99.93 methane by GC-FID) calculated in CSMHYD program [*Sloan*, 1998]. The dashed lines indicate the geotherms for different heat flux values modified from. Ground temperature for subaerial conditions is taken −15°C. Bottom water temperature is taken −0.5°C. Thicknesses of subaerial permafrost (10.5 ka) and present time submarine permafrost are modified from *Portnov et al.* [2014]. *Y* axes on the figures show depths in meters belowground surface (m bgs) and below the seafloor (m bsf). Permafrost-related GHSZ is shown for subaerial conditions (10.5 ka) and subsea conditions (present time) depending on different heat flux: (a) 0.07 W m^{-2}, (b) 0.06 W m^{-2}, and (c) 0.07 W m^{-2}.

offshore Yamal Peninsula in August 2013 revealed bottom water temperatures varying from +0.5°C in shallow water (~15 m) to −1°C in deeper water (>30 m). The Arctic and Antarctic Research Institute (AARI) database collates bottom water temperature data since the 1920s (Figure 1b), supporting these new water mass measurements. According to the AARI data and temperature-depth measurements, bottom water temperature at 40 m water depth varies from 0 to −1.0°C. Thus, shelf flooding in postglacial times has led to a significant temperature increase from −15°C to −0.5°C [*Pavlidis et al*., 1998; *Rozenbaum and Shpolyanskaya*, 2000; *Smith and Burgess*, 2000].

Such distinct bottom water warming impacts on the subsea permafrost through thermal diffusion and eventually propagates through to the top of the gas hydrate stability zone (GHSZ) [*Sloan*, 1998]. *Portnov et al.* [2014] notes that an equilibrium temperature distribution within subsea permafrost establishes itself at ~1000 years after flooding (geothermal heat flux and bottom water temperature are taken as 0.07 W m^{-2} and −0.5°C, respectively). Differences in geothermal heat flux values significantly affect the depth path of freezing during the global sea regression and what remains from subsea permafrost thickness and GHSZ at the present time (Figure 2) [*Portnov et al*., 2014; *Taylor et al*., 2013; *Nicolsky et al*., 2012]. A few existing heat flux records from the South Kara Sea shelf show values ranging from 0.054 to 0.076 W m^{-2} [*Khutorskoy and Podgornyh*, 2010].

Such variation implies contrasting scenarios of permafrost and GHSZ evolution. Under the elevated geothermal heat flux (0.07 W m^{-2}), continuous permafrost at 40 m below sea level (bsl) will have completely thawed and the corresponding GHSZ should have completely diminished (Figure 2a). Under the moderate geothermal heat flux (0.06 W m^{-2}) ~100 m thick permafrost can still exist at 40 m bsl water depths. However, its lower boundary is too shallow to provide temperatures low enough for gas hydrates to be stable (Figure 2b). Finally, under 0.05 W m^{-2} heat flux scenario permafrost may still be >150 m thick, providing intrapermafrost and subpermafrost GHSZ in the study area (Figure 2c).

The major part of subsea permafrost detected by drilling is limited by ~20 m isobath [*GEOS*, 1997; *Portnov et al*., 2013]. However, even in the shallow water depths permafrost does not occur in every drilled borehole location, indicating that permafrost degraded heterogeneously over an extended shallow shelf area [*GEOS*, 1997; *Melnikov and Spesivtsev*, 1995]. Heterogeneous conditions of degrading permafrost are favorable for a local release of methane, which has been previously sealed by permafrost and/or gas hydrates [*Shakhova et al*., 2013].

3. Methods

3.1. Sampling Sites and Techniques

Field studies carried out by I.S. Gramberg VNIIOkeangeologia in 2012 and 2013 on R/V "*Neotrazimy*" and R/V "*Ivan Petrov*" included HRS profiling and site-specific geological sampling in the South Kara Sea (Figure 1a).

Approximately 700 km of HRS lines were acquired using the EdgeTech 3100 SB-216S subbottom chirp operated at a frequency range of 2–16 kHz. The chirp provides at best subbottom penetration of ~80 m and vertical resolution of 20 cm in clays under calm weather conditions. The instrument setting used included a 2–15 kHz sweep with 20 ms pulse duration and 0.25 s pulse range. Depending on seabed properties and sea roughness during the cruise, the data provide ~0.5–1 m vertical resolution and 10–30 m penetration.

Based on very distinct bottom relief features we selected two well-pronounced PLFs for our detailed studies. PLF 1 is located at the West Yamal shelf in the northern part of Baydaratskaya Bay, while PLF 2 is located northward from PLF 1 (Figure 1a) above a deep structure considered for oil and gas potential [*Stupakova*, 2011].

For gravity coring we used a 250 kg weight stand with a 3 m long core barrel. Target sites for sediment coring were selected on top of PLFs and in adjacent areas. Reference core sites are located on a relatively featureless seafloor. The core positioning has been controlled by using the high-precision acoustic positioning and underwater navigation system HiPAP 350P-5. Recovered sediment cores were visually described and examined for evidence of gas or the presence of ice. Subsamples for geochemical analysis were taken from the intervals 27–33 cm, 97–103 cm, and 147–153 cm.

3.2. Laboratory Processing of Samples

For all subsampling performed on board we used conventional headspace gas extraction techniques. We placed a 100 mL plug of sediment into a 270 mL vial, containing 120 mL of distilled water. Hermetically

sealed vials with previously injected argon were shaken for 5 h at 400 rpm. These gas samples were stored in 15 mL crimped vials and afterward delivered to the onshore laboratory. Samples for the extraction of high molecular weight hydrocarbons were stored on board in ziplock bags in the freezer at a temperature of −23°C.

Postcruise laboratory studies included gas chromatography–flame ionization detector (GC-FID) analyses of hydrocarbon gases and HMW hydrocarbons. Stable isotopic measurements were performed by ISOLAB (Netherlands). For compositional analyses of hydrocarbon gases we used a gas chromatograph Shimadzu GC 2014 with flame-ionized detector equipped with wide bore capillary column Restek Rt-Aluminia bond 50 m × 0.53 mm × 10 μm. We tested the precision of the instrument by following the multiple injection method described by *Grob and Barry* [2004]. Ten injections of a standard sample, containing 10 ppm of various C_1–C_5 gases, showed an uncertainty of ±0.1 ppm. The precision of the method (repeatability) was tested by multiple runs of the identical analytical routine applied to the same sample. Estimated repeatability of the method is ±3%. This discrepancy is inevitably involved in all GC-FID results provided below.

Sample processing for analysis of HMW hydrocarbons started with a high-vacuum freeze drying and subsequent powdering of a weighted quantity. For subtracting C_{10}–C_{35} hydrocarbons we facilitated the Gerhardt SOX416 extraction system. As an internal standard we used 20 mL of squalane solution with concentration of 7.5 mg/L. After the extraction procedure we used a rotary evaporator for concentrating the samples. Gas chromatographic analyses were carried out using Shimadzu GC 2014c equipped with AOC-20i autosampler.

The $\delta^{13}C_{CH4}$ analyses were done on an Agilent 6890N GC interfaced to a Finnigan Delta S isotope ratio mass spectrometer (IRMS). For the δD measurements an Agilent 7890A GC interfaced to a MAT 253 IRMS was used. The results of carbon and hydrogen isotope measurements are expressed in terms of δ values in per mil relative to Pee Dee belemnite and SMOW standards, respectively.

4. Results

4.1. Seismic Data

HRS line spacing (~30–40 km) precludes statistically reliable estimates of the total number of PLFs that exist in the study area. However, HRS data reveal four distinct circular features, rising ~5–9 m above the surrounding seafloor at ~40 m water depth, which we classify as PLFs. Furthermore, seismic imagery reveals PLFs as acoustically transparent domes, bounded by dipping seismic reflector sequences on their flanks (Figures 1c and 1d). We subdivide these mounds into two contrasting sites: PLF1 and PLF2 (Figures 1c and 1d). PLF 1 incorporates three distinct PLFs with diameters ranging between 100 and 1000 m. PLF 2 is a smaller, yet marked, circular, singular feature with a diameter of only ~70 m. Layered sediments fill up the moats surrounding PLFs (Figures 1c and 1d).

4.2. Bottom Sediments

We recovered four sediment cores at the study area PLF 1 (Table 1). At the sites PLF_1_1 and PLF_1_6, we obtained relatively long sediment cores (210 cm and 232 cm, respectively). The sediments consisted of olive-gray bioturbated mud, which is very common for Holocene deposits throughout the Kara Sea [*Polyak et al.*, 2002]. No visible evidence existed for gas bubbling in the cores during onboard examinations. At sites PLF_1_3 and PLF_1_5, located on the flanks of the PLF, gravity core penetration was limited (Figure 3). After three repeated coring attempts at each location, two short sediment sections of 37 cm and 33 cm were retrieved. The sediments consisted of gray-colored clays with minor silt and sand contributions without indications of frozen sediment. Sediments were unable to be recovered from the top of the mound (planned coring site PLF_1_4), indicating an extremely hard seafloor and/or possibly frozen sediments. Away from the PLFs, in the outer northwestern part of the Baydaratskaya Bay, Holocene marine sediments show very high linear sedimentation rates (>100 cm/kyr) [*Polyak et al.*, 2002; *Stein et al.*, 2004].

At the PLF 2 sites, soft sediments consisted of homogeneous bioturbated olive-gray to dark gray mud (Figure 3). Only core PLF_2_4 differed, showing a 27 cm thick layer of black sediments with a very distinct hydrogen sulphide smell in its lower part. Such sediments are indicative for sulphate reduction in the sulphate-methane transition zone, beneath in which increased methane concentrations exist [*Coffin et al.*, 2008].

Table 1. Location, Water Depths, and Recovery of Gravity Cores

		Latitude		Longitude			
Study Site	Core	Minimum	Deg	Minimum	Deg	Water Depth (m)	Penetration (cm)
PLF_1	PLF_1_1	69	58.40366°N	65	18.15229°E	40	210
	PLF_1_3	69	57.87086°N	65	20.08569°E	38	37
	PLF_1_4	69	57.73125°N	65	20.55832°E	35	-
	PLF_1_5	69	57.43890°N	65	21.80662°E	39	33
	PLF_1_6	69	57.63263°N	65	21.06688°E	41	232
PLF_2	PLF_2_1	74	54.88789°N	69	43.11647°E	35	43
	PLF_2_2	74	54.92308°N	69	43.22785°E	30	99
	PLF_2_3	74	54.92806°N	69	43.24986°E	31	106
	PLF_2_4	74	54.94881°N	69	43.29353°E	36	115
	PLF_2_5	74	54.97575°N	69	43.38956°E	37	112
	PLF_2_6	74	54.99016°N	69	43.41372°E	36	187

4.3. Hydrocarbon Gases

Analyses of interstitial gases from within and around the PLFs reveal significant differences in the composition and concentration of gaseous hydrocarbons (C_1–C_5).

Methane concentrations are higher in all samples taken from PLF 2 if compared to samples taken from the same intervals in sediment cores from PLF 1 (Figure 4). PLF 1 methane concentrations at 30 cm subbottom

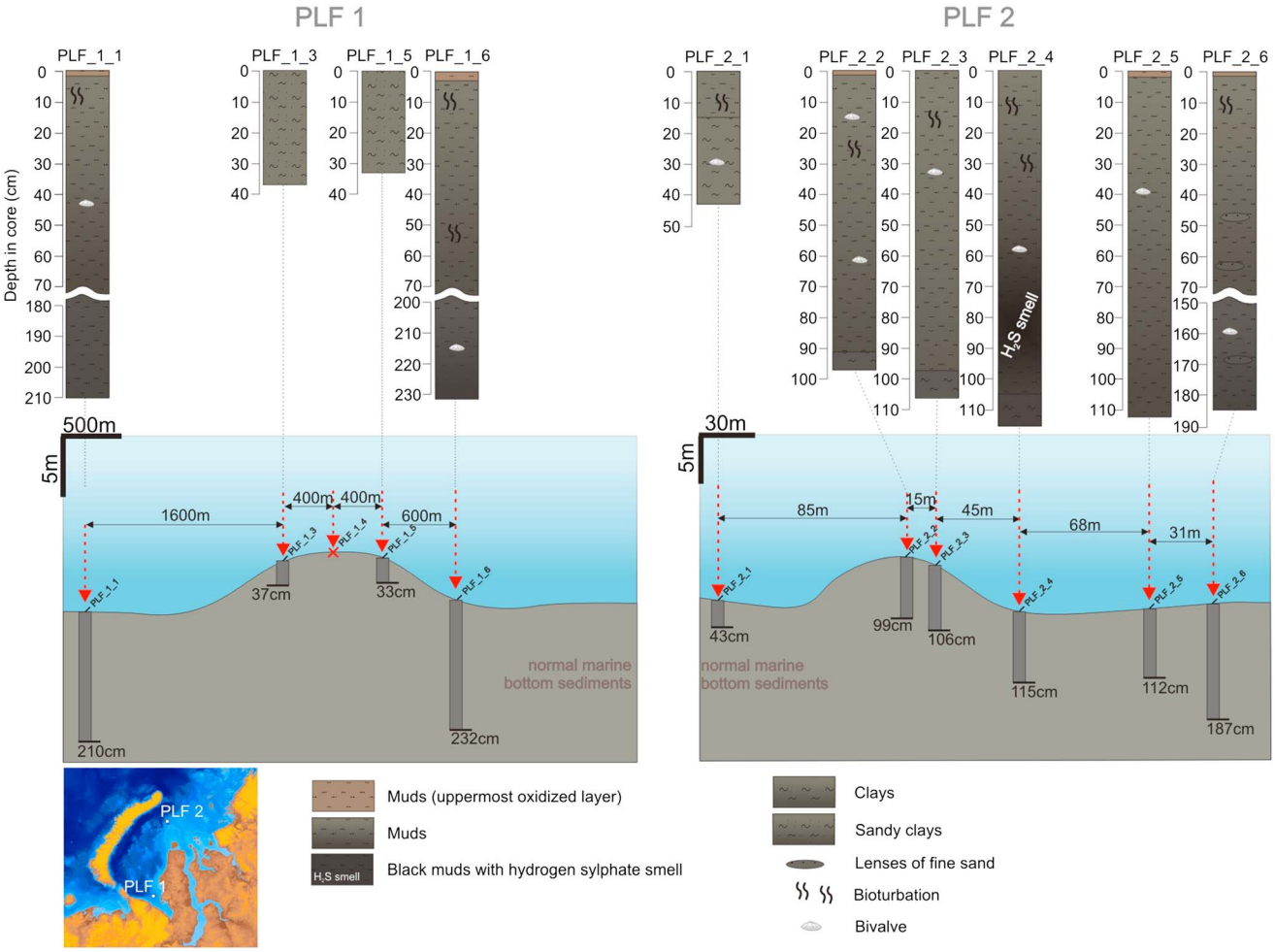

Figure 3. Locations, lengths, and lithology of investigated sediment cores.

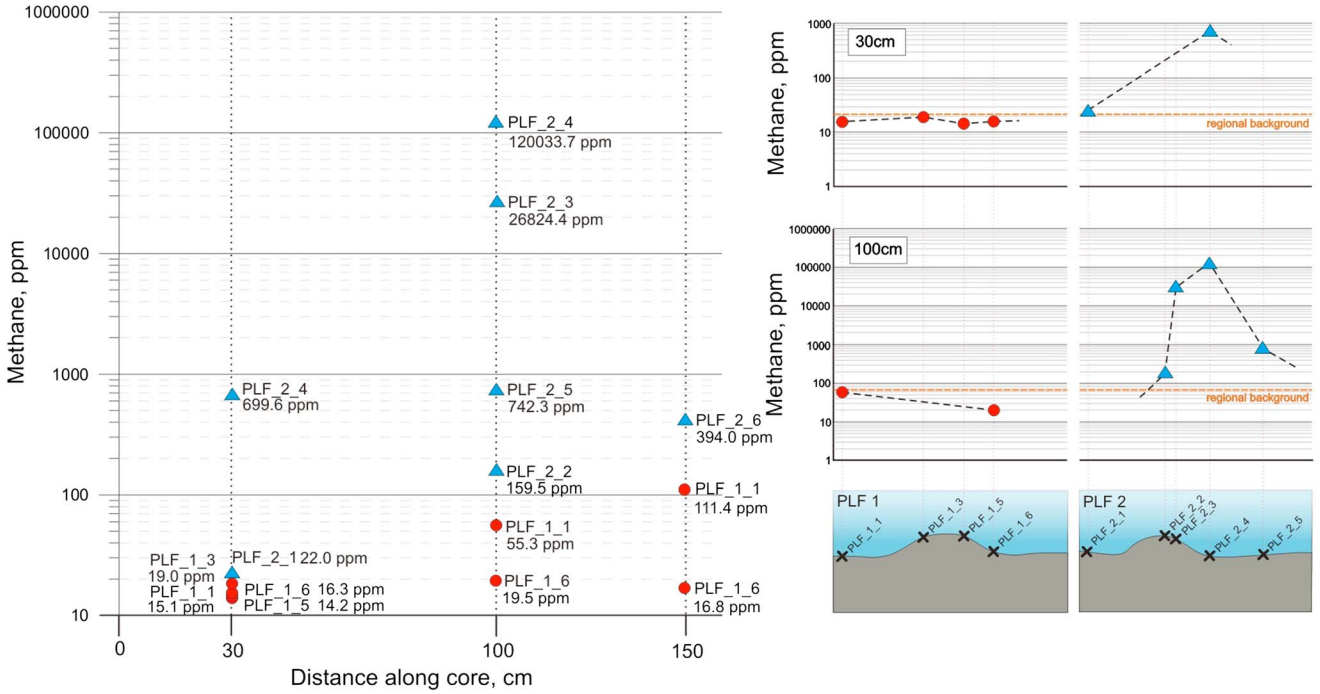

Figure 4. Methane concentrations in samples showing interstitial gas from sediment cores collected from PLF 1 and PLF 2. The red dots indicate the samples from PLF 1. The blue triangles show the samples from PLF 2.

depth (sbd) are relatively low and vary from 14.2 ppm to 19.0 ppm. In contrast, PLF 2 samples from 30 cm sbd show higher-methane concentrations reaching 22.0 ppm and 699.6 ppm, respectively (Figure 4). Similarly, methane concentrations at 100 cm sbd in the samples from PLF 1 do not exceed 55.3 ppm, while samples from PLF 2 show much higher concentrations, i.e., from 159.5 ppm to 120,033.7 ppm, respectively. Of particular note are methane concentrations in cores taken from PLF 2, which are more than 3 times higher at 150 cm sbd than in sediment cores from PLF 1 (Figure 4).

Results of grid-pattern surface geochemical investigations, performed by I.S. Gramberg VNIIOkeangeologia, documented regional background methane concentrations in the bottom sediments of the South Kara Sea shelf of less than 22 ppm at 30 cm and 60 ppm at 100 cm sbd, respectively. Thus, most of the samples taken from PLF 1 show concentrations lower than estimated background values. However, methane concentrations at PLF 2 show markedly higher values well above regional background levels (Figure 4). Site PLF_2_4 shows the highest-methane concentration of >120,000 ppm at 100 cm sbd, but we did not observe any gas flares in the water column using our chirp data (2–16 kHz). However, this is not conclusive because flares may actually be recorded if one uses a higher-frequency (>18 kHz) echo sounder [*Nikolovska et al*., 2008; *Weber et al*., 2014].

Anomalously high-methane concentrations (core PLF_2_4) are found at the PLF transition zone, between the flanks and the surrounding featureless seafloor. For example, methane concentrations around PLF 2 decrease from >120,000 to 26,824.4 ppm. Conversely, on the very top of the PLFs, methane concentrations are considerably lower at 159.5 ppm (Figure 4).

The fraction of total hydrocarbon gas versus wet gas [*Abrams and Dahdah*, 2011] reveals a consistent pattern with three groups of samples (Figure 5). The first group represents samples with moderate-methane concentrations (from 22.8 ppm to 743.9 ppm) and low wet gas fraction (from 0.007 to 0.04), indicative for background values. The second group shows anomalous samples with extremely high methane concentrations (>10,000 ppm) but low wet gas fraction (Figure 5). Finally, the third group represents fractionated samples characterized by low methane (<100 ppm) and increased wet gas fraction compared to background values (Figure 5). Such a pattern may be a result of differential volatile loss of methane compared to its heavier homologs, leading to a wet gas [*Abrams*, 2005].

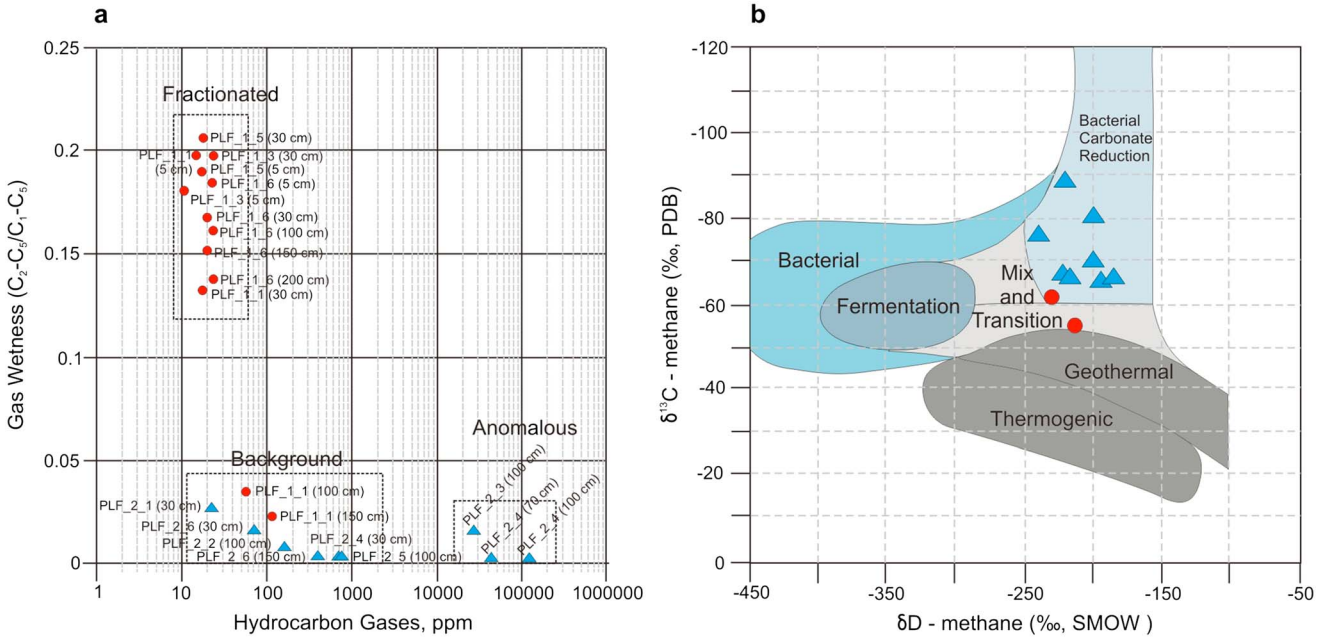

Figure 5. (a) Total extracted interstitial hydrocarbon gases (C_1–C_5) versus wet gas fraction (C_2–C_5/C_1–C_5) from sediment cores collected within PLF 1 and PLF 2. (b) CD diagram for gas genetic classifications [*Whiticar*, 1999]. The red dots show the samples from PLF 1. The blue triangles show the samples from PLF 2.

4.4. Stable Isotopes

We present the isotope data in standard δ notation (expressed in per mil) plotted on a carbon-deuterium diagram (Figure 5b) [*Whiticar*, 1999].

All studied samples demonstrate $\delta^{13}C_{CH4}$ values ranging from −55.1‰ to −88.0‰ and δD_{CH4} values ranging from −175‰ to −246‰, which is consistent with a biogenic source of methane. However, one group of samples shows a relatively heavy isotope composition of carbon from −55.1‰ to 62.1‰ (Figure 5). We suggest that these methane samples may reflect either secondary isotopic effects (substrate depletion and methane oxidation) [*Whiticar*, 1999] or a presence of trace amounts of thermogenic methane from deeper hydrocarbon sources.

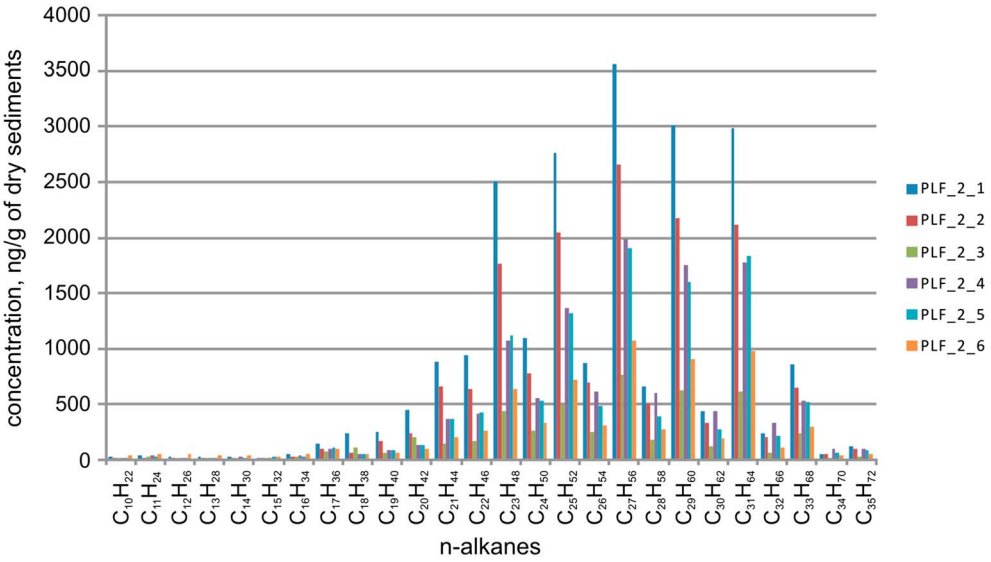

Figure 6. Distribution of *n*-alkanes extracted from the sediment core from PLF 2.

Table 2. High Molecular Weight Hydrocarbon Indexes Calculated for the Samples From PLF 2[a]

		n-Alkanes							
		$\Sigma C_{10}–C_{40}$	$\Sigma C_{10}–C_{15}$	$\Sigma C_{16}–C_{24}$	$\Sigma C_{25}–C_{35}$				
Core	TOC, %	ng/g Dry Sediments				Overall CPI	$CPI_{10–15}$	$CPI_{16–24}$	$CPI_{25–35}$
PLF_2_1	1.01	22,339	174.92	6,594.19	15,569.89	3.32	0.94	1.26	4.91
PLF_2_2	1.18	16,089.43	92.76	4,453.5	11,543.17	3.44	0.73	1.35	4.6
PLF_2_4	0.56	5,019.38	104.51	1,498.23	3,416.63	2.41	1.3	0.88	3.71
PLF_2_5	1.63	12,563.57	124.19	2,825.36	9,614.02	2.75	1.14	1.19	3.22
PLF_2_6	0.87	6,991.69	236.39	1,797.28	4,958.02	2.79	0.94	1.17	3.8

[a]CPI = carbon preference index; overall CPI = (ΣOdds $C_{11–33}$ + ΣOdds $C_{13–35}$)/2(ΣEvens $C_{11–35}$); $CPI_{10–15}$ = 0,5*((C_{11} + C_{13} + C_{15})/(C_{10} + C_{12} + C_{14}) + (C_{11} + C_{13} + C_{15})/(C_{12} + C_{14} + C_{16})); $CPI_{16–24}$ = 0,5*((C_{17} + C_{19} + C_{21} + C_{23})/(C_{18} + C_{20} + C_{22} + C_{24}) + (C_{17} + C_{19} + C_{21} + C_{23})/(C_{20} + C_{22} + C_{24} + C_{26})); and $CPI_{25–35}$ = 0,5*((C_{25} + C_{27} + C_{29} + C_{31} + C_{33} + C_{35})/(C_{24} + C_{26} + C_{28} + C_{30} + C_{32} + C_{34}) + (C_{25} + C_{27} + C_{29} + C_{31} + C_{33} + C_{35})/(C_{26} + C_{28} + C_{30} + C_{32} + C_{34} + C_{36}).

4.5. High Molecular Weight Hydrocarbons (*n*-Alkanes)

PLF 2 is located above a geological structure promising for oil and/or gas exploration [*Stupakova*, 2011]. The migration of gases from deeper sources to the subseabed may therefore play a role within this area. We studied HMW hydrocarbons in order to identify migrated thermogenic compounds and ascertain the nature of recent organic matter [*Abrams*, 2005; *Abrams and Dahdah*, 2011]. Shallow bottom sediments in gas leakage sites, fueled by deep and mature hydrocarbons, often show associated anomalies of high molecular weight hydrocarbons, including *n*-alkanes [*Hood et al*., 2002; *Lorenson et al*., 2014; *Abrams*, 2005]. Thus, we consider it essential to provide *n*-alkane data to constrain whether methane leakage is related to mature hydrocarbons.

Analyses of *n*-alkanes show that higher molecular compounds prevail in all studied cores (Figure 6). The concentration of long-chain *n*-alkanes (C_{25}–C_{35}) varies from 4958.0 to 15,569.9 ng/g of dry sediment, whereas concentrations of *n*-alkanes with shorter chains vary from 92.8 to 174.9 ng/g (C_{10}–C_{16}) and from 1498.2 to 6594.2 ng/g (C_{16}–C_{24}) of dry sediments (Figure 6 and Table 2). Bulk *n*-alkane fraction changes from 5019.4 to 22,339.0 ng/g of dry sediments (Table 2).

The carbon preference index (overall CPI), which defines the ratio between odd and even *n*-alkanes, varies from 2.35 to 3.39, indicating a predominance of odd molecules (Table 2). $CPI_{16–24}$ and $CPI_{25–35}$ also show a prevalence of odd *n*-alkanes (except for $CPI_{16–24}$ in core PLF_2_4) (Table 2). Even C_{10}–C_{15} *n*-alkanes dominate in the samples from PLF_2_1, PLF_2_2, and PLF_2_6, which is reflected in low $CPI_{10–15}$ (Table 2). However, the C_{10}–C_{15} group demonstrates insufficiently small concentrations if compared to C_{16}–C_{24} and C_{25}–C_{35} (Figure 6 and Table 2). Thus, the contribution of even C_{10}–C_{15} *n*-alkanes to the bulk composition is negligible.

5. Discussion

5.1. Beaufort Sea Shelf Pingo-Like Features

Early studies proposed a model for the origin of PLFs based on the morphological similarity and spatial proximity of terrestrial pingos and PLFs [*Shearer et al*., 1971; *Mackay*, 1998]. These models suggested that PLFs on the Beaufort Sea shelf initially grew under subaerial conditions during the LGM sea level lowstand before ~19 ka, after which they became submerged during the Holocene transgression [*Fairbanks*, 1989; *Shearer et al*., 1971]. However, several points contradict this hypothesis. Considering that the PLFs on the Beaufort Sea shelf are located in water depths ranging from 30 to 80 m, they should have been exposed to increased seawater temperatures for as long as ~14 to ~9 kyr [*Fairbanks*, 1989]. Moreover, open-water wave actions would have mechanically eroded the PLFs over time. Both thermal and mechanical influences of the Holocene flooding should have therefore alterated the original PLF's shape, potentially causing collapsed structures or wave undercuts at their seaward parts. However, neither early studies [*Shearer et al*., 1971] nor recent studies that involved multibeam mapping, high-resolution seismic imaging, and remotely operated vehicle survey [*Paull et al*., 2007] reported observations that would support such processes.

Table 3. Comparison of PLFs and Onshore Pingos From Different Regions

Criteria		Beaufort Sea PLFs	Pechora Sea PLFs	South Kara Sea PLFs	Tuktoyaktuk Pingos
Diameter	minimal	25 m	50 m	70 m	10 m
	average	400 m	-	-	20–50 m
	maximal	-	600 m	1000 m	600 m
Height	minimal	4 m	2 m	5 m	3 m
	average	10–30 m	-	-	-
	maximal	40 m	25 m	10 m	70 m
Water depths		25–70 m	50–100 m	35–45 m	onshore features
Distribution		clusters, pairs, and single features	clusters, pairs, and single features	clusters and single features	clusters, pairs, and single features
Seismic signatures		zones demonstrating lack of internal structure	acoustically transparent zones	acoustically transparent zones	-
Specific features (gas seeps, moats, collapsed structures, etc.)		negative relief moats; gas seeps at the crests of the structures	negative relief moats, overpressured gas accumulations	negative relief moats	collapsed structures, dilation cracks, and wave-eroded structures
Gas compositions		predominantly methane	-	predominantly methane	-
Isotope compositions		$d^{13}C = -76.6\%$ and $dD = -179\%$ (biogenic)	-	$d^{13}C = -55.1\%$ to -88% and dD = from -179% to -246% (biogenic)	-

Alternative hypotheses suggest that the development of PLFs occurred in submarine conditions, at places where small lakes or a freshwater supply existed for some time [*Shearer et al*., 1971]. Sediments containing freshwater in the pore space of sediments are more prone to freezing in submarine environments. Thus, the hydrostatic pressure of expelled pore water and frost heaving might trigger upheaval [*Shearer et al*., 1971; *Mackay*, 1998]. These scenarios require steady bottom water temperatures below the freshwater freezing point and a well-sealed freshwater lens protected from mixing with seawater. Alternatively, submarine groundwater flow from onshore may add freshwater to an aquifer that can prevent salinization of nearshore marine sediments after an ocean transgression [*Post et al*., 2013]. Calculations of *Shearer et al.* [1971] showed that even in cases of persistently cold bottom water temperatures (below 0°C) the average time required for the 0°C isotherm to reach the lower boundary of a water-saturated lens is approximately 5 kyr. Thus, a very specific and impermeable lithology is required to keep the freshwater lens from mixing with seawater for such a long time, especially during the early stages of the Holocene transgression when wave action contributed to infiltration of seawater into soils in coastal marine environments. However, submarine discharge of groundwater can potentially cause an intrusion of freshwater into the shallow subsurface resulting in a change of the sediment pore water freezing point and, thus, PLF growths [*Frederick and Buffett*, 2015].

More recent studies have discovered methane gas seeps at the crests of many PLFs on the Beaufort Sea shelf [*Paull et al*., 2007] (Table 3). Earlier hypotheses describing the marine inundation of terrestrial pingos therefore do not help to explain these extensive methane discharges. A scenario proposed by *Paull et al.* [2007] suggests that PLFs might be formed by decomposing permafrost-associated gas hydrates undergoing a thermal equilibration with seawater. At the top of the submerging GHSZ both methane bubbles and pure ice may exist. A transition from gas hydrate via dissociation to gas bubbling where ice may still exist provokes an expansion of the sediment matrix driving the extrusion of ice- and gas-saturated sediments toward the seafloor [*Paull et al*., 2007]. Methane bubbles reaching the seafloor will discharge to the bottom water, with the relief of stress within the formerly gas-saturated layer and mass transfer triggering subsidence of surrounding zones and the development of moats [*Paull et al*., 2007], similar to what has been observed in this South Kara Sea study area.

5.2. Formation of Pingo-Like Features in Areas of Thawing Subsea Permafrost

Acoustically transparent zones exist in both regions containing PLFs, as seen on HRS lines (Figures 1c and 1d). However, even HRS profiles do not allow for distinguishing between ice-saturated and gas-saturated sediments. PLF 1 has concentrations of hydrocarbon gases ubiquitously below the regional background value (19.5–55.3 ppm at 100 cm sbd), while PLF 2 represents extremely high concentrations (159.5–120,033.7 ppm at 100 cm sbd) that are much higher than the background value (60 ppm). Gas saturation might therefore induce acoustic transparency in PLF 2.

The unsuccessful gravity coring at the top of PLF 1 suggests that it is capped by a hard layer, contrary to PLF 2 where core penetration into the sediment using the same sampling technique was easily achieved (Figure 3). There is no evidence for boulders or carbonate crusts in the area around PLF 1 that could potentially hinder core penetration, although the hard bottom may be explained by the presence of frozen sediments.

PLF 1 is the largest (~1000 m in diameter and 7 m high) seabed feature within the adjacent study area and in relation to PLF 2. Moats surrounding PLFs have been previous reported from the shallow (30–80 m bsl) Beaufort Sea shelf adjacent to Tuktoyaktuk Peninsula and from the Pechora Sea shelf [*Bondarev et al*., 2002; *Rokos*, 2008] but also from areas with terrestrial pingos [*Paull et al*., 2007; *Mackay*, 1998] (Table 3). Taking into account the possibility of frozen sediments within the mound, and structural similarities between PLF 1 and those studied in the Beaufort and Pechora Seas, we suggest a similar origin for the South Kara Sea PLFs.

PLF 2 also exhibits a well-pronounced seabed expression (Figure 1c), but compared to PLF 1 is smaller in diameter, and singular conic-shaped. Bottom sediments of both PLF 2 and PLF 1 do not show any mudflow structures or breccia within the imaged seafloor and recovered materials. We therefore exclude the possibility of a mud volcano.

Anomalous methane concentrations were documented at PLF 2. PLF 1 lacks even background levels of methane concentrations, consistent with the presence of indurated sediments and the likely presence of ice. Frozen sediments prevent significant in situ methane production and may block any ascending flux of gas coming from deeper subsurfaces.

A low wet gas fraction in the samples from both PLFs points toward a microbial origin of gas. We interpret the increased wet gas ratio in a group of samples from PLF 1 (Figure 5a) to be a result of differentiation caused by higher volatile loss of methane compared to its heavier homologs. In general, absolute concentrations of homologs C_2–C_5 do not exceed background values and therefore do not support a focused discharge of mature gaseous hydrocarbons from a deep subsurface.

Isotope compositions of carbon and hydrogen measured in methane samples reflect a distinct microbial signature showing a good agreement with the results of GC-FID analyses (Figure 5). Two samples from PLF 2 show relatively heavy isotope compositions of carbon (Figure 5b). At the same time, they do not demonstrate any leaps in concentrations of methane and/or its heavier homologs, thus pointing toward methane that has been influenced by oxidation and/or depletion of its substrate.

The ubiquitously low content of organic matter in the bottom sediments of PLF 2 (total organic carbon (TOC) varied from 0.52% to 1.69% with an average 1.04%), as well as on the featureless seafloor (from 0.1 to 1.55% with an average 0.92%), restricts vigorous release of microbial in situ methane, pointing toward a migration of microbial gas from greater depth. However, no sites have so far been observed that show such a migration on the surrounding flat seafloor.

Results of the HMW hydrocarbons study at PLF 2 show a predominance of long chain ($>C_{23}$) odd *n*-alkanes. Thermocatalytic decomposition of organic matter during the catagenesis that is responsible for generation of oil and natural gas produces odd and even homologs in equal proportion, whereas live systems, especially plants, produce mostly odd-chained compounds [*Didyk et al*., 1978]. Thus, a predominance of odd compounds, expressed in CPI >2 (Figure 6 and Table 2), strongly indicates a prevalence of terrigenous organic matter in our samples, which is typical of the Kara Sea shelf [*Boucsein et al*., 1999]. In comparison, a thermogenic signature is usually reflected by a CPI <1 [*Abrams*, 2005]. Our data set suggests the absence of a thermogenic signature within C_{16}–C_{24} and C_{25}–C_{35} ranges (Table 2). The C_{10}–C_{15} range demonstrates a lower CPI, varying from 0.73 to 1.30 (Table 2). However, short-chain *n*-alkanes are present only in insignificant quantities (Figure 6 and Table 2). Results of the HMW study at PLF 2 therefore demonstrate no evidence for expulsion of mature hydrocarbons from a deep subsurface to the shallow sediments, suggesting that the observed seepage shows no relations to mature deep-sourced hydrocarbons. However, drilling data are needed to give an insight into deeper subsurface process.

Models of subsea permafrost evolution (Figure 2) suggest possible scenarios for the origin of PLF 1 and PLF 2. First, observations show that PLF1 and PLF 2 have a similar appearance on acoustic images and that the PLFs occur in similar water depths (~40 m).

The modeled boundary of the lower permafrost shows a significant upward shift in response to the geothermal heat flux (Figure 2). A permafrost evolution scenario based on an elevated heat flux of ~0.07 W m^{-2} [*Khutorskoy and Podgornyh*, 2010] corresponds with other empirical observations [*Portnov et al*., 2014]. These heat flux would have caused a thawing and dissociation of the permafrost and GHSZ at water depths of ~40 m, an area where PLFs exist today (Figure 2a).

PLF 1 does not indicate a migration of hydrocarbon gases from deeper sources or pressurized buildups caused by growing gas accumulations. It is surprising that PLF 1 is not covered by marine sediments, because high sedimentation rates (27–159 cm/kyr) have been reported from the Kara Sea for the Holocene [*Polyak et al*., 2000; *Stein et al*., 2004]. Furthermore, the velocity of the Yamal Current, flowing to the northeast along the western slope of the Yamal Peninsula, is ~1 cm/s at 40 m water depth [*Zatsepin et al*., 2010], which may not be high enough to prevent sedimentation of silt and clay. This may suggest that PLF 1 has grown more recently and thus not yet buried.

Onshore pingos, as well as the Beaufort Sea PLFs, demonstrate more solid-ice concentrations compared to surrounding permafrost [*Mackay*, 1998; *Paull et al*., 2007]. Pure ice requires significantly more energy to melt than frozen sediments due to the larger latent heat value for pure ice relative to the bulk latent heat value of frozen sediments [*Farouki*, 1982; *Sass et al*., 1971]. Thus, low bottom water temperatures (−0.5°C in the South Kara Sea) and high ice content may allow for a better preservation of PLFs than relic subsea permafrost.

High concentrations of hydrocarbon gases at PLF 2 cannot originate from local microbial methane production alone. Additional gas from deeper source must therefore be considered. The modeling results (Figure 2) support gas transfer from thawed subsea permafrost and dissociating gas hydrates. Focused gas leakage in the area occurs in an otherwise low in situ methane production environment as documented by low regional background values (Figure 4). A PLF formation associated with melting of both permafrost and gas hydrates is therefore very likely for the South Kara Sea shelf. We suggest that PLF 2 developed during one of the three following stages of subsea permafrost and gas hydrate evolution: stage 1—GHSZ and permafrost exist; stage 2—GHSZ disappeared, permafrost and gas-saturated layer exist; and stage 3—GHSZ disappeared, discontinuous permafrost exists (Figure 2). Previous field studies [*Portnov et al*., 2013] and modeling results using available heat flux data [*Khutorskoy and Podgornyh*, 2010; *Portnov et al*., 2013] provide evidence for a discontinuous permafrost in water depths >20 m. The studied PLFs are located in water depths of ~40 m and therefore have most likely reached stage 3.

At stage 1, the mechanism envisioned by *Paull et al.* [2007], where GHSZ was still preserved in the South Kara Sea shelf, might take place. Ongoing thermal equilibration of permafrost during transgression of the shelf post-LGM would have caused the GHSZ to largely disappear leading to stage 2. At this stage, pressurized gas below the continuous permafrost can eventually extrude ice- and methane-saturated materials from the former intrapermafrost GHSZ to the seabed. The high heat flux (0.07 W m^{-2}) below the permafrost results in a further upward shift of the permafrost base. The more the permafrost thaws, the more methane accumulates beneath it, thus driving the pinch out of thinning permafrost. The high heat flux values and our observations support extensive permafrost degradation on the South Kara Sea shelf. Therefore, we suggest that PLF started to form during the transition from stage 2 to stage 3, when a thin, but still continuous, permafrost transformed into a discontinuous layer with locally significant gas storage below (Figure 2a).

6. Conclusions

Pingo-like features (PLFs) exist across the South Kara Sea in ~40 m water depth. One PLF (PLF 2) connects to biogenic gas from deeper sources. Integrated geochemical and geophysical studies suggest that the PLFs evolved after the Last Glacial Maximum and during the Holocene sea level transgression that flooded extensive areas of the Arctic continental shelves. The formation of one PLF (PLF 2) is directly linked to the thawing of subsea permafrost and decomposition of permafrost-related gas hydrates. High accumulations of biogenic methane create the necessary forces to push the remaining frozen layers upward. We speculate that PLF 1 is either a relict-submerged terrestrial pingo or a PLF lacking the necessary underlying methane accumulations. More detailed grid-pattern HRS and drill site investigations are needed to determine the complex distribution patterns of the South Kara Sea PLFs.

Acknowledgments
All data used in this paper as well as detailed description of geochemical and geophysical methods are available upon request from the authors. This work was partly supported by the Research Council of Norway throughout its Centers of Excellence funding scheme, project 223259. The field research was supported by the Federal Subsoil Resources Management Agency of Russia (object 70-113: "Regional geologic-geophysical explorations at Yamal sector of the South Kara Sea shelf"). We would like to thank Boris Vanshtein, Georgy Cherkashev, and Svyatoslav Usenkov for their advice and recommendations during the data collection, laboratory processing, and preparation of the manuscript. We also thank anonymous reviewers and Editor Bryn Hubbard for constructive comments that greatly improved the manuscript.

References

Abrams, M. A. (2005), Significance of hydrocarbon seepage relative to petroleum generation and entrapment, *Mar. Pet. Geol.*, *22*(4), 457–477, doi:10.1016/j.marpetgeo.2004.08.003.

Abrams, M. A., and N. F. Dahdah (2011), Surface sediment hydrocarbons as indicators of subsurface hydrocarbons: Field calibration of existing and new surface geochemistry methods in the Marco Polo area, Gulf of Mexico, *AAPG Bull.*, *95*(11), 1907–1935, doi:10.1306/03211110130.

Aubry, M.-P., J. A. Van Couvering, N. Christie-Blick, E. Landing, B. R. Pratt, D. E. Owen, and I. Ferrusquia-Villafranca (2009), Terminology of geological time: Establishment of a community standard, *Stratigraphy*, *6*(2), 100–105.

Bauch, H. A., T. Mueller-Lupp, E. Taldenkova, R. F. Spielhagen, H. Kassens, P. M. Grootes, J. Thiede, J. Heinemeier, and V. V. Petryashov (2001), Chronology of the Holocene transgression at the North Siberian margin, *Global Planet. Change*, *31*(1–4), 125–139, doi:10.1016/S0921-8181(01)00116-3.

Bogoyavlenskiy, V. (2014a), Threat of catastrophic gas blowouts from the Arctic permafrost zone. Yamal and Taimyr craters. Part 1, *Oil Drill.*, *9*, 13–18.

Bogoyavlenskiy, V. (2014b), Threat of catastrophic gas blowouts from the Arctic permafrost zone. Yamal and Taimyr craters. Part 2, *Oil Drill.*, *10*, 4–8.

Bondarev, V., S. Rokos, D. Kostin, A. Dlugach, and N. Polyakova (2002), Underpermafrost accumulations of gas in the upper part of the sedimentary cover of the Pechora Sea, *Geol. Geophys.*, *43*(7), 587–598.

Boucsein, B., K. Fahl, M. Siebold, and R. Stein (1999), Quantity and quality of organic carbon in surface sediments of the Ob and Yenisei estuaries and adjacent coastal areas: Marine productivity vs. terrigenous input, *Ber. Polarforschung*, *300*, 116–126.

Brothers, L. L., P. E. Hart, and C. D. Ruppel (2012), Minimum distribution of subsea ice-bearing permafrost on the U.S. Beaufort Sea continental shelf, *Geophys. Res. Lett.*, *39*, L15501, doi:10.1029/2012GL052222.

Coffin, R., L. Hamdan, R. Plummer, J. Smith, J. Gardner, R. Hagen, and W. Wood (2008), Analysis of methane and sulfate flux in methane-charged sediments from the Mississippi Canyon, Gulf of Mexico, *Mar. Pet. Geol.*, *25*(9), 977–987, doi:10.1016/j.marpetgeo.2008.01.014.

Collett, T. S., M. W. Lee, W. F. Agena, J. J. Miller, K. A. Lewis, M. V. Zyrianova, R. Boswell, and T. L. Inks (2011), Permafrost-associated natural gas hydrate occurrences on the Alaska North Slope, *Mar. Pet. Geol.*, *28*(2), 279–294, doi:10.1016/j.marpetgeo.2009.12.001.

Delisle, G. (2000), Temporal variability of subsea permafrost and gas hydrate occurrences as function of climate change in the Laptev Sea, Siberia, *Polarforschung*, *68*, 221–225.

Didyk, B. M., B. R. T. Simoneit, S. C. Brassell, and G. Eglinton (1978), Organic geochemical indicators of palaeoenvironmental conditions of sedimentation, *Nature*, *272*(5650), 216–222.

Fairbanks, R. G. (1989), A 17,000-year glacio-eustatic sea level record: Influence of glacial melting rates on the Younger Dryas event and deep-ocean circulation, *Nature*, *342*, 637–642.

Farouki, O. (1982), Thermal properties of soils, *Tech. Rep.*, Hanover, N. H.

Fleming, K., P. Johnston, D. Zwartz, Y. Yokoyama, K. Lambeck, and J. Chappell (1998), Refining the eustatic sea-level curve since the Last Glacial Maximum using far- and intermediate-field sites, *Earth Planet. Sci. Lett.*, *163*(1–4), 327–342, doi:10.1016/S0012-821X(98)00198-8.

Frederick, J. M., and B. A. Buffett (2014), Taliks in relict submarine permafrost and methane hydrate deposits: Pathways for gas escape under present and future conditions, *J. Geophys. Res. Earth Surf.*, *119*, 106–122, doi:10.1002/2013JF002987.

Frederick, J. M., and B. A. Buffett (2015), Effects of submarine groundwater discharge on the present-day extent of relict submarine permafrost and gas hydrate stability on the Beaufort Sea continental shelf, *J. Geophys. Res. Earth Surf.*, *120*, 417–432, doi:10.1002/2014JF003349.

GEOS (1997), *Baydaratskaya Bay Environmental Conditions. The Basic Result of Studies for the Pipeline "Yamal-Center" Underwater Crossing Design*, 432 pp., GEOS, EPS "Eco-System library", Moscow.

Grob, R., and E. Barry (2004), *Modern Practice of Gas Chromatography*, 4th ed., John Wiley, Hoboken, N. J.

Hood, K. C., L. M. Wenger, O. P. Gross, and S. C. Harrison (2002), Hydrocarbon systems analysis of the northern Gulf of Mexico: Delineation of hydrocarbon migration pathways using seeps and seismic imaging, in *Surface Exploration Case Histories: Applications of Geochemistry, Magnetics, and Remote Sensing*, *AAPG Stud. Geol. 48 and SEG Geophys. Ref. Ser. 11*, edited by D. Schumacher and L. A. LeSchack, pp. 25–40, Am. Assoc. of Petrol. Geol., Tulsa, Okla.

Hovland, M., A. G. Judd, and R. A. Burke Jr. (1993), The global flux of methane from shallow submarine sediments, *Chemosphere*, *26*(1–4), 559–578, doi:10.1016/0045-6535(93)90442-8.

Hu, K., D. Issler, Z. Chen, and T. Brent (2013), Permafrost investigation by well logs, and seismic velocity and repeated shallow temperature surveys, Beaufort-Mackenzie Basin, 33 pp., Natural Resources Canada/Ressources Naturelles Canada, doi:10.4095/293120.

Jakobsson, M., et al. (2014), Arctic Ocean glacial history, *Quat. Sci. Rev.*, *92*, 40–67, doi:10.1016/j.quascirev.2013.07.033.

Judd, A. G., and M. Hovland (2007), *Seabed Fluid Flow: The Impact on Geology, Biology and the Marine Environment*, 492 pp., Cambridge Univ. Press, New York.

Khimenkov, A., and A. Brushkov (2003), *Oceanic Cryolithogenesis*, 336 pp., Nauka, Moscow.

Khutorskoy, M. D., and L. V. Podgornyh (2010), Geothermics of the Arctic basin—The problems and solutions. Geothermal field and the Arctic shelf oil and gas bearing, *Monit. Sci. Technol.*, *1*(1), 6–26.

Levitan, M. A., M. V. Bourtman, L. L. Demina, V. V. Krupskaya, E. M. Sedykh, and M. Y. Chudetsky (2004), History of Holocene sedimentation in the southern Kara Sea, *Lithol. Miner. Resour.*, *39*(6), 566–579, doi:10.1023/b:limi.0000046959.42527.71.

Lorenson, T., F. Wong, P. Dartnell, and R. Sliter (2014), Greenhouse gases generated from anaerobic biodegradation of natural offshore asphalt seepages in Southern California, *Geo Mar. Lett.*, doi:10.1007/s00367-014-0359-1.

Majorowicz, J., J. Šafanda, and K. Osadetz (2011), Gas hydrates stability and the dynamics of taliks in the Mackenzie Delta, Canada, in *Proceedings of the 7th International Conference on Gas Hydrates*, edited, pp. 1–15, Heriot-Watt Univ., Edinburgh, Scotland.

Mackay, J. R. (1998), Pingo growth and collapse, Tuktoyaktuk Peninsula area, western Arctic coast, Canada: A long-term field study, *Géographie Physique et Quaternaire*, *52*(3), 271–323, doi:10.7202/004847ar.

Melnikov, V., and V. Spesivtsev (1995), *Engineering-Geological Conditions of Barents and Kara Sea Shelves*, Nauka, Novosibirsk, Russia.

Moskvitch, K. (2014), Mysterious Siberian crater attributed to methane, *Nature*, doi:10.1038/nature.2014.15649.

Nicolsky, D. J., V. E. Romanovsky, N. N. Romanovskii, A. L. Kholodov, N. E. Shakhova, and I. P. Semiletov (2012), Modeling sub-sea permafrost in the East Siberian Arctic shelf: The Laptev Sea region, *J. Geophys. Res.*, *117*, F03028, doi:10.1029/2012JF002358.

Nikolovska, A., H. Sahling, and G. Bohrmann (2008), Hydroacoustic methodology for detection, localization, and quantification of gas bubbles rising from the seafloor at gas seeps from the eastern Black Sea, *Geochem. Geophys. Geosyst.*, *9*, Q10010, doi:10.1029/2008GC002118.

Osterkamp, T. E., G. C. Baker, W. D. Harrison, and T. Matava (1989), Characteristics of the active layer and shallow subsea permafrost, *J. Geophys. Res.*, *94*(C11), 16,227–16,236, doi:10.1029/JC094iC11p16227.

Paull, C., W. Ussler, S. R. Dallimore, S. M. Blasco, T. D. Lorenson, H. Melling, B. E. Medioli, F. M. Nixon, and F. A. McLaughlin (2007), Origin of pingo-like features on the Beaufort Sea shelf and their possible relationship to decomposing methane gas hydrates, *Geophys. Res. Lett.*, *34*, L01603, doi:10.1029/2006GL027977.

Pavlidis, Y. A., A. S. Ionin, F. A. Sherbakov, N. N. Dunaev, and S. L. Nikiforov (1998), *The Arctic Shelf. Late-Quaternary Geological History as a Framework for the Future Prognosis*, 184 pp., GEOS, Moscow.

Polyak, L., M. Levitan, V. Gataullin, T. Khusid, V. Mikhailov, and V. Mukhina (2000), The impact of glaciation, river-discharge and sea-level change on late Quaternary environments in the southwestern Kara Sea, *Int. J. Earth Sci.*, *89*(3), 550–562, doi:10.1007/s005310000119.

Polyak, L., M. Levitan, T. Khusid, L. Merkulin, and V. Mukhina (2002), Variations in the influence of riverine discharge on the Kara Sea during the last deglaciation and the Holocene, *Global Planet. Change*, *32*(4), 291–309, doi:10.1016/S0921-8181(02)00072-3.

Polyak, L., F. Niessen, V. Gataullin, and V. Gainanov (2008), The eastern extent of the Barents–Kara ice sheet during the Last Glacial Maximum based on seismic-reflection data from the eastern Kara Sea, *Polar Res.*, *27*(2), 162–174.

Portnov, A., A. J. Smith, J. Mienert, G. Cherkashov, P. Rekant, P. Semenov, P. Serov, and B. Vanshtein (2013), Offshore permafrost decay and massive seabed methane escape in water depths >20 m at the South Kara Sea shelf, *Geophys. Res. Lett.*, *40*, 3962–3967, doi:10.1002/grl.50735.

Portnov, A., J. Mienert, and P. Serov (2014), Modeling the evolution of climate-sensitive Arctic subsea permafrost in regions of extensive gas expulsion at the west Yamal shelf, *J. Geophys. Res. Biogeosci.*, *119*, 2082–2094, doi:10.1002/2014JG002685.

Post, V. E. A., J. Groen, H. Kooi, M. Person, S. Ge, and W. M. Edmunds (2013), Offshore fresh groundwater reserves as a global phenomenon, *Nature*, *504*(7478), 71–78, doi:10.1038/nature12858.

Rachold, V., D. Bolshiyanov, M. Grigoriev, H.-W. Hubberten, R. Junker, V. Kunitsky, F. Merker, P. Overduin, and W. Schneider (2007), Near-shore arctic subsea permafrost in transition, *Eos Trans. AGU*, *88*(13), 149–150, doi:10.1029/2007EO130001.

Rekant, P., and A. Vasiliev (2011), Distribution of subsea permafrost at the Kara Sea shelf, *Cryosphere Earth*, *XV*(4), 69–72.

Rekant, P., G. Cherkashev, B. Vanstein, and P. Krinitsky (2005), Submarine permafrost in the nearshore zone of the southwestern Kara Sea, *Geo Mar. Lett.*, *25*(2-3), 183–189, doi:10.1007/s00367-004-0199-5.

Rokos, S. (2008), Engineering-geological characteristics of near-surface areas of the anomaly high embedded pressure at the shelves of Pechora and Kara Seas, *Eng. Geol.*, *4*, 22–28.

Rokos, S., and G. Tarasov (2007), Gas-saturated sediments of South Kara Sea Bays and gulfs, *Bull. Stud. Quat. Period*, *67*, 66–75.

Rokos, S., A. Dlugach, A. Loktev, D. Kostin, and S. Kulikov (2009), Permafrost of the Pechora and the Kara Seas: Genesis, structure and conditions of its distribution, *Eng. Surv.*, *10*, 38–41.

Romanovskii, N. N., A. V. Gavrilov, A. L. Kholodov, G. P. Pustovoit, F. Niessen, H. Kassens, and H. W. Hubberten (1998), Map of predicted offshore permafrost distribution on the Laptev Sea shelf, in *7th International Conference on Permafrost*, *Collect. Nordicana*, edited by M. Allard and A. G. Lewkowicz, pp. 967–972, Center for Northern Studies, Univ. of Laval.

Romanovskii, N. N., H. W. Hubberten, V. E. Romanovsky, and A. L. Kholodov (2003), Permafrost evolution under the influence of long-term climate fluctuations and glacio-eustatic sea-level variation: Region of Laptev and East Siberian Seas, Russia, paper presented at 8th International Conference on Permafrost, Swets & Zeitlinger, Zurich, Switzerland.

Romanovskii, N. N., H. W. Hubberten, A. V. Gavrilov, V. E. Tumskoy, and A. L. Kholodov (2004), Permafrost of the East Siberian Arctic shelf and coastal lowlands, *Quat. Sci. Rev.*, *23*(11–13), 1359–1369, doi:10.1016/j.quascirev.2003.12.014.

Romanovskii, N. N., H. W. Hubberten, A. V. Gavrilov, A. A. Eliseeva, and G. S. Tipenko (2005), Offshore permafrost and gas hydrate stability zone on the shelf of East Siberian Seas, *Geo Mar. Lett.*, *25*(2-3), 167–182, doi:10.1007/s00367-004-0198-6.

Rozenbaum, G., and N. Shpolyanskaya (2000), Late Cenozoic history of Arctic permafrost and tendency of its evolution, *Sci. World*, Moscow.

Ruppel, C. (2007), Tapping methane hydrates for unconventional natural gas, *Elements*, *3*, 193–199.

Sass, J. H., A. H. Lachenbruch, and R. J. Munroe (1971), Thermal conductivity of rocks from measurements on fragments and its application to heat-flow determinations, *J. Geophys. Res.*, *76*(14), 3391–3401, doi:10.1029/JB076i014p03391.

Shakhova, N., I. Semiletov, I. Leifer, A. Salyuk, P. Rekant, and D. Kosmach (2010), Geochemical and geophysical evidence of methane release over the East Siberian Arctic shelf, *J. Geophys. Res.*, *115*, C08007, doi:10.1029/2009JC005602.

Shakhova, N., et al. (2013), Ebullition and storm-induced methane release from the East Siberian Arctic shelf, *Nat. Geosci.*, *7*, 64–70, doi:10.1038/ngeo2007.

Shearer, J. M., R. F. Macnab, B. R. Pelletier, and T. B. Smith (1971), Submarine pingos in the Beaufort Sea, *Science*, *174*(4011), 816–818, doi:10.1126/science.174.4011.816.

Sherbakov, V., V. Motichko, and V. Konstantinov (2010), *Estimation of Background Geological Conditions of Nearshore Area and Coastal Zone at South-West Kara Sea for Monitoring of Bowels, Rep. 504.4:556351(268.52)*, 270 pp., VNIIOkeangeologia, Saint-Petersburg, Russia.

Sloan, E. D. (1998), *Clathrate Hydrates of Natural Gases*, CRC Press, Taylor & Francis Group, New York.

Smith, S., and M. Burgess (2000), Ground temperature database for Northern Canada, *Open File Rep. 3954*, 28 pp., Geol. Surv. of Canada.

Stein, R., et al. (2004), Arctic (palaeo) river discharge and environmental change: Evidence from the Holocene Kara Sea sedimentary record, *Quat. Sci. Rev.*, *23*(11–13), 1485–1511, doi:10.1016/j.quascirev.2003.12.004.

Stupakova, A. (2011), Structure and petroleum potential of the Barents-Kara Shelf and adjacent territories, *Oil Gas Geol.*, *6*, 99–115.

Svendsen, J. I., V. Gataullin, J. Mangerud, and L. Polyak (2004), The glacial history of the Barents and Kara Sea Region, *Dev. Quat. Sci.*, *2*, 369–378, doi:10.1016/S1571-0866(04)80086-1.

Taylor, A. E., S. R. Dallimore, P. R. Hill, D. R. Issler, S. Blasco, and F. Wright (2013), Numerical model of the geothermal regime on the Beaufort Shelf, arctic Canada since the Last Interglacial, *J. Geophys. Res. Earth Surf.*, *118*, 2365–2379, doi:10.1002/2013JF002859.

Weber, T. C., L. Mayer, K. Jeram, J. Beaudoin, and Y. Rzhanov (2014), Acoustic estimates of methane gas flux from the seabed in a 6000 km^2 region in the Northern Gulf of Mexico, *Geochem. Geophys. Geosyst.*, *15*, 1911–1925, doi:10.1002/2014GC005271.

Whiticar, M. J. (1999), Carbon and hydrogen isotope systematics of bacterial formation and oxidation of methane, *Chem. Geol.*, *161*(1), 291–314.

Yakushev, V. S. (2009), *Natural Gas and Gas Hydrates in the Permafrost*, 192 pp., GAZPROM VNIIGAZ, Moscow.

Zatsepin, A. G., E. G. Morozov, V. T. Paka, A. N. Demidov, A. A. Kondrashov, A. O. Korzh, V. V. Kremenitsliy, S. G. Poyarkov, and D. M. Soloviev (2010), Circulation in the southwestern part of the Kara Sea in September 2007, *Oceanology*, *50*(5), 643–656.